LABORATORY INVESTIGATIONS OF THE MECHANISMS OF GROUNDWATER SEEPAGE EROSION AND PIPING IN COHESIVE SOILS

By

RACHEL GAYLE FELICE

Bachelor of Science in Biosystems Engineering

Oklahoma State University

Stillwater, Oklahoma

2010

Submitted to the Faculty of the
Graduate College of the
Oklahoma State University
in partial fulfillment of
the requirements for
the Degree of
MASTER OF SCIENCE
December, 2012

LABORATORY INVESTIGATIONS OF THE

MECHANISMS OF GROUNDWATER SEEPAGE

EROSION AND PIPING IN COHESIVE SOILS

Thesis Approved:

Dr. Garey Fox

Thesis Adviser

Dr. Glenn Brown

Dr. Rifat Bulut

ACKNOWLEDGEMENTS

I would sincerely like to thank Dr. Fox. As my advisor he has taught me, led me and encouraged me throughout this entire process. In the classroom he has provided the ability to tackle some of the most difficult analyses and outside the classroom has proved instrumental in overcoming obstacles with his guidance.

I would also like to thank Dr. Glenn Brown for his encouragement and mentorship throughout my college career.

Thank you to Dr. Rifat Bulut and Dr. Glenn Wilson for your guidance and support of this research.

Thank you to Wayne Kiner and the Biosystems Engineering Lab for their knowledge, skill and support.

Several graduate students have contributed to this research. I especially would like to thank Taber Midgley, Abdul-Sahib Al-Madhhachi, Rebecca Chavez and Erin Daly. I would also like to thank undergraduate students Mohammed Rahi, Louis Steigerwald and Rebecca Purvis for their support of this project.

Finally, I wish to thank my husband Robert Felice for his unfailing support and encouragement through this entire process.

Name: RACHEL GAYLE FELICE

Date of Degree: DECEMBER, 2012

Title of Study: LABORATORY INVESTIGATION OF THE MECHANISMS OF GROUNDWATER SEEPAGE EROSION AND PIPING IN COHESIVE SOILS

Major Field: BIOSYSTEMS ENGINEERING

Abstract: Seepage and soil piping are two mechanisms that can cause streambank erosion and failure. Groundwater seepage can cause erosion either by undercutting or "pop-out" failure. The objective of the seepage study was to utilize a constant-head soil box packed with sandy loam soils at prescribed bulk densities (1.30-1.70 Mg m^{-3}) and an outflow face at 90°. Bulk density controlled the mechanism of seepage erosion/failure. For both soils, tension failures occurred at densities less than 1.60 Mg m^{-3} and undercutting was observed for densities 1.60 Mg m^{-3} or greater. Data from experiments was used to calibrate SEEP/W to determine pore-water pressures. SLOPE/W utilized the pore-water pressures to determine stability. SLOPE/W only incorporates pore-water pressure effects in factor of safety calculations; therefore, the model was unsuccessful at predicting a failure. Seepage gradient forces may play a more prominent role in streambank and hillslope instability, and this mechanism should be incorporated into stability models. In addition, soil pipe experiments were conducted and flow and internal erosion data were derived for two soils packed at uniform bulk densities but different initial moisture contents. Soils included were clay loam (Dry Creek) and sandy loam (Cow Creek). Initial gravimetric moisture contents (MC) were 10, 12 and 14% for Dry Creek soil and 8, 12, and 14% for Cow Creek soil. A 1-cm diameter rod created the horizontal pipe. A constant head was maintained; flow rates and sediment concentrations were measured from the pipe outlet. Submerged jet erosion tests (JETs) derived erodibility parameters. Flow rates from the box experiments calibrated the deterministic model. The influence of the initial MC of the packed soil was apparent with some pipes (8% MC) expanding so fast that limited data was collected. The deterministic model estimated equivalent flow rates, but had difficulty matching observed sediment concentrations when pipes rapidly expanded by internal erosion. The submerged JETs predicted similar erodibility coefficients compared to the deterministic model for the more erodible cases (8 and 12% MC), but not for the less erodible cases (14% MC).

TABLE OF CONTENTS

Chapter Page

LIST OF TABLES

Table Page

LIST OF FIGURES

Figure Page

CHAPTER I

INTRODUCTION

Sediment is known to be one of the most prominent pollutants of surface water. Streambank erosion is known to be a major source of sediment in streams and rivers and can contribute up to 80% of the total sediment yield in certain watersheds (Wilson et al., 2008). Sedimentation of streams and lakes is becoming a significant problem in places like Oklahoma where residents rely heavily on lake water storage to protect communities from large flood events.

Groundwater seepage is one of the mechanisms that cause streambank erosion and failure. Seepage erosion occurs when a hydraulic gradient exists in a porous medium that eventually exits at the face of a streambank or hillslope at sufficient exit velocities to mobilize sediment (Tomlinson and Vaid, 2000). Groundwater can seep through soil and cause erosion either by undercutting or “pop-out” failure (Chu-Agor et al., 2008a). Undercutting occurs when seepage entrains particles and transports them from the soil mass, creating an undercut and eventual mass failure. “Pop-out” failure is due to slope instability and results in a mass failure before any undercutting occurs. Chu-Agor et al. (2008a) suggested that bulk density contributed to the type of seepage erosion observed

in sands and loamy sand soils. Undercuts were observed to occur at a higher bulk density while “pop-out” failures occurred at lower densities, suggesting a critical density. That controls the failure mode.

Another mechanism for streambank erosion is soil piping. Flow through an open macropore, i.e. soil pipe, may lead to internal erosion of the pipe walls which can result in streambank failure, gullies, and embankment failure (Fox and Wilson, 2010). The pipe flow, particle detachment, and sediment transport processes involved are complex. Internal erosion of a soil pipe is typically described by the classic excess shear stress equation (Fox and Wilson, 2010). This shear stress equation was developed for and typically applied to overland flow which involves a two-dimensional planar surface. For a water-filled soil pipe, these forces act on the two-dimensional radial surface of the pipe and along its length, thereby enlarging the pipe circumference as a function of length along the soil pipe. For conditions in which a soil pipe extends through a reservoir's embankment, as the pipe enlarges, the "infinite" head of the reservoir can maintain water-filled conditions (Bonelli et al., 2006). Flow rates increase as the pipe enlarges, thereby providing a positive feedback mechanism that result in more rapid internal erosion. Soil pipe enlargement progresses rapidly to the point that the soil above can no longer be supported and the soil pipe collapses resulting in an embankment breach or mature gully formation.

Another important pipe flow erosion mechanism involves pipe clogging as a result of sediment transport limitations. When internal erosion exceeds the sediment transport capacity, pipe clogging can occur. It has been postulated by Pierson (1983) and Uchida et al. (2001) that clogging may result in pressure build ups that can cause sudden

mass failures of hillslopes (e.g., landslides and debris flows). In laboratory soil pipeflow experiments, Wilson (2009, 2011) noted that clogging resulted in surges in pipeflow. Such turbulent flow conditions resulted in high sediment concentrations and rapid expansion of the pipe diameter. Numerical simulations of these experiments (Wilson and Fox, 2013) indicated that the clogging, even for periods as short as 0.1 s, produced almost instantaneous pressure buildups within the soil pipes.

1.1 Objectives

The primary objectives of this research were to (i) investigate seepage and piping erosion mechanisms in cohesive streambanks using a laboratory soil box and (ii) utilize the data to determine the predictive capability of commonly used models for streambank/hillslope stability and internal erosion. The seepage study utilized a constant-head soil box packed with sandy loam soils at uniform bulk densities (1.30-1.70 Mg m^{-3}), an outflow face at 90°, and a dry antecedent moisture content to simulate seepage in streambanks. The piping study utilized the same constant-head soil box to conduct soil pipe experiments and derive flow and internal erosion data for two soils packed at uniform bulk densities but different initial moisture contents. Both studies evaluated the ability of a model to predict laboratory observations.

1.2 Organization of Thesis

Chapter II presents research with objectives to (i) induce seepage in two sandy loam soils at different densities to determine the demarcation point at which undercutting occurs versus tension failures, (ii) compare results to a previous study by Chu-Agor et al.

(2008a), and (iii) evaluate a seepage and slope stability model (SEEP/SLOPE) using data from the seepage experiments in terms of its ability to predict failure.

Chapter III presents research with the objectives of (i) induce piping and internal erosion in two cohesive soils from different streambanks packed at different initial moisture contents and quantify flow and erosion rates during the erosion process, and (ii) use data from piping and internal erosion experiments to assess ability of a deterministic pipe flow model to correctly predict pipe flow and erosion rates.

Chapter IV presents the general conclusions and suggestions for future work.

.

CHAPTER II

UNDERCUTTING AND TENSION FAILURES BY GROUNDWATER SEEPAGE: LABORATORY EXPERIMENTS ON COHESIVE SOILS

2.1 Abstract

Groundwater seepage can lead to the erosion and failure of streambanks and hillslopes by two mechanisms: (1) tension or "pop-out" failure due to the seepage force exceeding the soil shear strength or (2) undercutting and eventual mass failure. Previous research on these mechanisms has been limited to noncohesive and low cohesion soils such as sands and loamy sands. This study utilized a constant-head soil box packed with sandy loam soils at prescribed bulk densities (1.30-1.70 Mg m^{-3}), an outflow face at 90°, and a dry antecedent moisture content to simulate seepage through soils. Bulk density of the two different soil types controlled the mechanism of seepage erosion/failure. For both soils, tension failures occurred at bulk densities of less than 1.60 Mg m^{-3} and undercutting was observed for bulk densities 1.60 Mg m^{-3} or greater. Undercutting shapes in less cohesive soils were more focused at the center of the soil box with particle entrainment that resulted in less wide and deeper undercuts. However, undercutting in the sandy loam soils were much wider and typically extended the entire distance across the face of the soil box. Inflow and outflow data from laboratory experiments was used to calibrate

SEEP/W to determine pore-water pressures in the soil. SLOPE/W then utilized the pore-water pressure analysis to determine soil stability. SLOPE/W only incorporated pore-water pressure effects as driving forces in factor of safety calculations. Therefore, the model was unsuccessful at predicting failure. Seepage gradient forces may play a more prominent role in the instability of streambanks and hillslopes, and this mechanism should be incorporated into stability models.

Keywords: Failure, Pore-Water Pressure, Seepage, Streambank Stability, Undercutting.

2.2 Introduction

Sediment is known to be one of the most prominent pollutants of surface water. In many places across the nation and around the world, it has been found that streambank erosion is contributing significantly to sedimentation in reservoirs. One of the less understood mechanisms of this erosion is groundwater movement, specifically seepage (Crosta and di Prisco, 1999). Seepage erosion occurs when a hydraulic gradient exists in a porous medium that eventually exits at the face of a streambank or hillslope at sufficient velocities to mobilize sediment (Tomlinson and Vaid, 2000). Knowledge and consideration of all potential streambank erosion processes are required to completely understand this dynamic and complex system.

Groundwater can seep through soil and cause erosion and failure either by undercutting or “pop-out” failure (Chu-Agor et al., 2008a, 2008b). Undercutting occurs when seepage either at the bank toe or within a conductive soil layer entrains and transports particles, creating an undercut and eventual mass failure. Pop-out failure is due

to slope instability and results in a mass failure before any undercutting occurs. Initial research by Chu-Agor et al. (2008a) suggested that bulk density predicted the type of seepage erosion observed in sands and loamy sands. Undercutting was observed to occur at a higher bulk density while pop-out failures occurred at lower densities, suggesting a critical density where undercutting is observed rather than pop-out failure.

While seepage and seepage erosion have been extensively studied, there are still many aspects that are not well understood. Seepage effects on pore-water pressures and seepage gradients are still being quantified. Streambanks can often be layered, or largely one soil type, and seepage erosion can happen in either case.

Seepage velocity is given by Darcy's Law:

$$v_s = \frac{K_{sat}}{n} i \tag{2-1}$$

where v_s is the seepage velocity, K_{sat} is the saturated hydraulic conductivity of the soil, i is the hydraulic gradient, and n is the porosity of the soil. Seepage influences the stability of streambanks, hillslopes, and embankments through increased soil pore-water pressure, seepage gradient forces, and seepage particle mobilization and undercutting (Fox and Wilson, 2010).

2.2.1 Increased Soil Pore-Water Pressure

Soil strength is often defined using the Mohr-Coulomb equation:

$$s = c' + (\sigma_n - u_w)\tan\phi' \tag{2-2}$$

where s is the shear strength, c' is the effective cohesion, ϕ' is the effective angle of internal friction, σ_n is the total normal stress, and u_w is the soil pore-water pressure

(Whitlow, 1983; Fredlund and Rahardjo, 1993). In unsaturated soils, matric suction has the effect of increasing the apparent cohesion of the soil, as described by Fredlund and Rahardjo (1993):

$$s = c' + (\sigma_n - u_w)\tan\phi' + (u_a - u_w)\tan\phi^b \tag{2-3}$$

where u_a is the soil pore-air pressure and ϕ^b is the angle indicating the rate of increase in the shear strength relative to matric suction and is generally between 10^o and 20^o. From these equations, an increase in pore-water pressure decreases the effective stress of the soil thereby decreasing the soil shear strength (Fox and Wilson, 2010).

2.2.2 Seepage Gradient Forces

Seepage forces acting on soil are proportional to the hydraulic gradient (*i*):

$$\tau_s = \rho g d i \tag{2-4}$$

where τ_s is the seepage stress, ρ is the density of the fluid, *g* is gravity, and *d* is the grain diameter. Several studies have incorporated this seepage force into equations for particle mobilization by seepage such as Lobkovsky et al. (2004) who modified the Shields number to include this seepage force.

2.2.3 Particle Mobilization and Undercutting

Tension or “pop-out” failures due to pore water pressure increases are easier to predict due to research conducted by Chu-Agor et al. (2008a). However, predicting erosion due to particle mobilization (i.e., entrainment in the seepage flow) remains

restricted. Seepage erosion occurring before massive bank slumping (Bradford and Piest, 1977) has been highlighted as a potential failure mechanism of streambanks, predominantly on the recession limb of the streamflow hydrographs (Fox et al., 2007; Wilson et al., 2007). When streambanks retain enough resistance to overcome pore water pressure effects, particle mobilization and undercutting can occur when the velocity of water exiting the bank face exceeds the critical shear stress (Chu-Agor et al., 2008a). As undercutting occurs, bank stability decreases exponentially (Wilson et al., 2007).

Chu-Agor et al. (2008a) focused only on sandy and loamy sand soils, however seepage undercutting has been observed in a range of soil types. Figure 2-1 shows undercutting at Goodwin Creek in Mississippi which is comprised of silt loam soil (Fox et al., 2007). Further research is needed to better understand undercutting processes. Unfortunately, a fully integrated variably saturated flow model with dynamic geometric and geotechnical capabilities is currently lacking and is required to predict the three-dimensional nature of seepage entrainment and undercutting (Fox and Wilson, 2010).

Figure 2-1. Undercutting at Goodwin Creek, Mississippi.

2.2.4 Objective

The objective of this research was to induce and evaluate seepage failure mechanisms using varying hydraulic conditions in more cohesive soils (i.e., reduced soil shear strength, seepage gradient forces, and seepage particle mobilization and undercutting). Also this research attempted to establish demarcation points for tension or pop-out failures by seepage gradient forces and compare them to results from less cohesive soils reported by Chu-Agor et al. (2008a), again investigating the three-dimensional nature of seepage particle mobilization and undercutting.

2.3 Methods and Materials

2.3.1 Physical Modeling

A section of streambank was modeled in the laboratory. Figure 2-2 shows the acrylic box used consisting of a water reservoir, a 0.10 m by 0.10 m focused screened inlet, and a 0.50 m by 0.50 m soil compartment. Soil was processed using a 4.75 mm (no. 4) sieve and moisturized to an antecedent moisture content between 5 and 10% before packing. Two different soils were used: sandy loam 1, SL1 (66% sand, 28% silt, 6% clay) and sandy loam 2, SL2 (72% sand, 13% silt, 15% clay), as classified based on the USDA soil texture classification. For all experiments, a cohesive clay was packed as the first layer in the soil block. The clay was packed as densely as possible in a 25 mm lift. SL1 was packed to bulk densities of 1.30, 1.45, 1.60 and 1.70 Mg m^{-3}. SL2 was packed to bulk densities of 1.30, 1.50 and 1.60 Mg m^{-3}. All experiments consisted of soil

blocks packed in 25 mm lifts to a height of 0.25 m, width of 0.50 m and depth of 0.25 m. The soil for all experiments was packed to a 90° angle in the box. Constant heads of 0.15, 0.25 and 0.35 m were maintained in the water reservoir using a Marriott bottle infiltrometer. Duplicate experiments were completed for each scenario which resulted in 24 experiments.

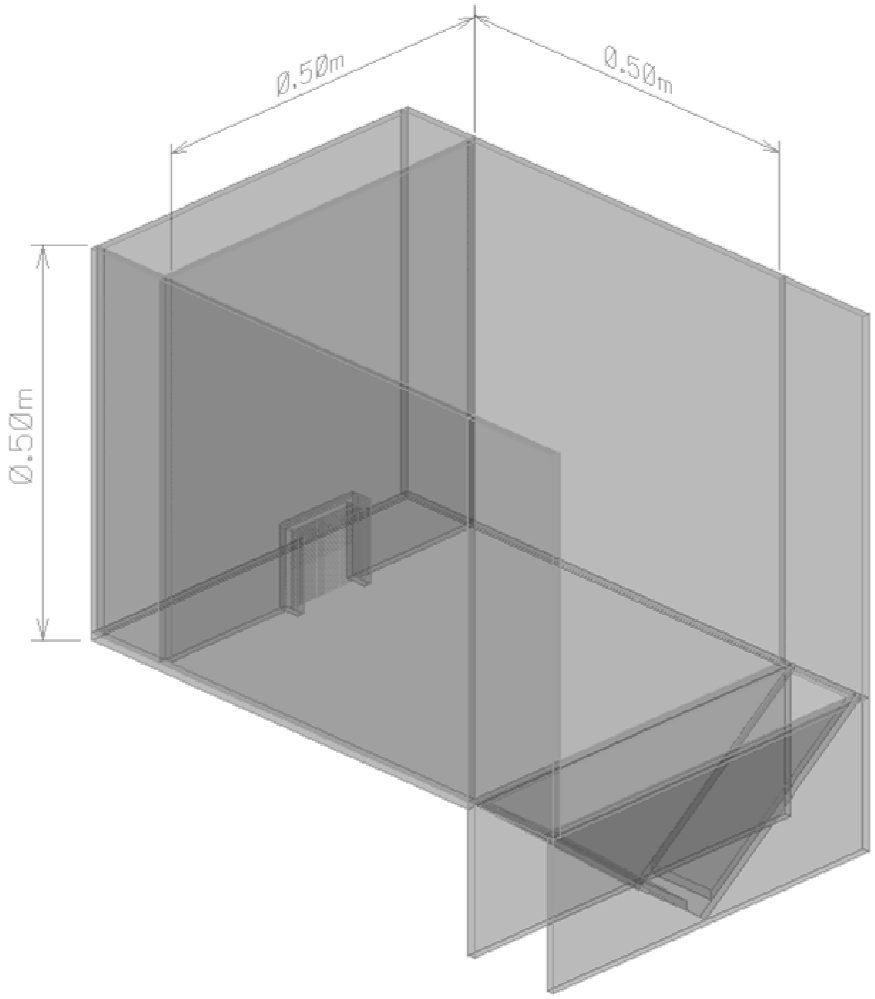

Figure 2-2. 3-Dimensional box used in laboratory experiments.

Data collected during experiments included water arrival at the bank face, the time of seepage erosion initiation, seepage erosion over time, and the eroded volume of the bank. Inflow and outflow were monitored using computer controlled scales and weights recorded every five seconds. A three-dimensional laser scanner (EScan Scanner, 3D Digital Corporation, Sandy Hook, CT) was used to obtain undercutting shapes. The scanner is a medium range scanning device with resolutions of 135 micrometers at a 300 mm scanning distance and 210 micrometers at a 650 mm scanning distance with a point density of 255 by 1000 points. For the experiments, all scans were manually captured within 650 mm of the bank face. Scanned images were recorded in XYZ coordinates as a point cloud. The XYZ coordinates were then used to create 2.0 mm square grids using an inverse to distance power algorithm (Chu-Agor et al., 2008a).

2.3.2 Numerical Modeling of Seepage and Stability

A subset of the laboratory experiments (SL1 for 1.45 and 1.60 Mg m^{-3} with imposed heads of 0.15 and 0.25 m) were numerically modeled. SEEP/W was used (GeoStudio 2004, Version 6.22) to simulate pore water pressures and cumulative fluxes across inflow and outflow boundaries, while SLOPE/W (GeoStudio 2004, Version 6.22) was used for slope stability analyses. Current versions of the model (GeoStudio 2012) cannot simulate seepage undercutting. However, if the model captured the prominent failure mechanisms observed during “pop-out” failures, then it would be able to predict a similar demarcation point for soils as observed in the laboratory.

SEEP/W is a finite element model of Richards' equation for two-dimensional variably-saturated flow (Krahn, 2004a). The flow domain was constructed to represent

the geometry of the box experiments with two distinct material regions: soil of interest (SL1 and SL2) and clay. Each region was then divided into 14.3 mm by 12.5 mm elements.

Assigning material properties in SEEP/W involves defining the water retention function, $\theta(h)$, and the hydraulic conductivity function, $K(h)$, where h is the soil-water pressure (Krahn, 2004a). The van Genuchten (1980) model was used to estimate $\theta(h)$, while RETC (van Genuchten et al., 1991) was used to estimate van Genuchten parameters for each soil at the density used in the laboratory experiments. SEEP/W can represent $K(h)$ by the van Genuchten (1980) model using parameters obtained from the water retention function and a saturated hydraulic conductivity value, K_{sat} (Chu-Agor et al., 2008b). The K_{sat} was obtained using falling head tests for each density and is discussed later in this section.

Calibration of the models was achieved by slightly adjusting K_{sat}. SEEP/W uses Dirichlet boundary conditions in which the hydraulic head is specified at a boundary. The initial conditions of the models matched those of the constant hydraulic head imposed on each experiment. A potential seepage review boundary condition for all the nodes was assigned at the drainage face. In SEEP/W, a potential seepage review boundary condition is used when neither the hydraulic head nor the discharge are known beforehand but instead must be computed by the model (Krahn, 2004a), as in the case of the drainage from the box face. A constant total head was used as the boundary condition at the inflow face. Boundary conditions and model set-up are shown in Figure 2-3.

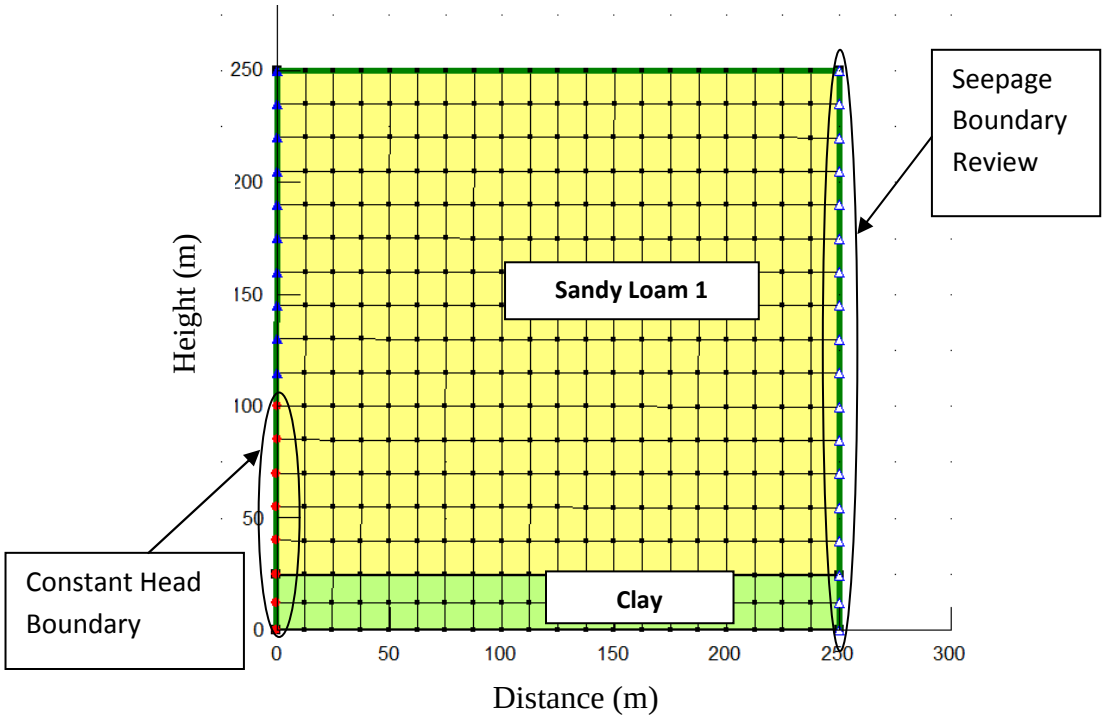

Figure 2-3. Model set-up dimensions and boundary conditions.

Transient simulations were run for each model and initial water tables were positioned at a level below the material regions. Initial water table settings were derived from the hydraulic function water content curve and moisture content of the soil used in laboratory experiments. Time steps depended on laboratory observations and each model was allowed to run well past failure times observed in the laboratory experiments.

SLOPE/W uses the theory of limit equilibrium of forces and moments to compute the factor of safety (*Fs*) against failure (Chu-Agor et al., 2008b). It discretizes a potential sliding mass into vertical slices and applies static equilibrium equations (Krahn, 2004b). The *Fs* is defined as the ratio of the resistive forces to the driving forces. The *Fs* is an index of the relative stability of a slope (Chu-Agor et al., 2008b).

SLOPE/W was used to analyze the stability of the streambank as simulated by the laboratory experiments. The stability modeling procedure had three components: (1) definition of the geometry and shape of the potential slip surface, (2) definition of the soil strength properties, and (3) definition of the soil-water pressure (Chu-Agor et al., 2008b). SEEP/W and SLOPE/W are integrated codes such that the geometry defined in SEEP/W is included in SLOPE/W. Soil strength parameters in the laboratory experiments were defined using Coulomb's equation. For an effective stress analysis, the shear strength is defined using equation (2-2) (Krahn, 2004b).

The Morgenstern and Price method was selected for computing *Fs*. This method satisfies both the moment and force equilibrium equations and can give accurate results for all practical conditions (Krahn, 2004b). The general limit equilibrium method uses:

$$X = E\lambda f(x) \tag{2-5}$$

where *f(x)* is the specified function, λ is the percentage of the specified function, *E* is the interslice normal force, and X_R and X_L are the interslice shear forces on either side of a slice. According to Chu-Agor et al. (2008b), the general limit equilibrium method then uses static equations 2-6, 2-7 and 2-8 to solve for the *Fs*, where *W* is the slice weight, *D* is the line load, β, *R*, *x*, *f*, *d*, and ω are the geometric parameters, and α' is the inclination of the base:

The summation of forces in a horizontal direction for each slice is used to compute the interslice normal force, *E* (equation 2-5). This equation is applied in an integration manner across the sliding mass (i.e., from left to right).

The summation of forces in a vertical direction for each slice is used to compute the normal force at the base of the slice, *N*, where *F* is either the moment or force equilibrium factor of safety:

$$N = \frac{W + \left(X_R - X_L\right) - \dfrac{c'\beta\sin\alpha' + u\beta\sin\alpha'\tan\phi'}{F}}{\cos\alpha' + \dfrac{\sin\alpha'\tan\phi'}{F}} \tag{2-6}$$

The summation of moments about a common point for all slices can be rearranged and solved for the moment equilibrium factor of safety, *Fm*.:

$$Fm = \frac{\sum\left(c'\beta R + \left(N - u\right)R\tan\phi'\right)}{\sum W - \sum Nf \pm \sum Dd} \tag{2-7}$$

The summation of forces in a horizontal direction for all slices, gives rise to a force equilibrium factor of safety, *Fs*:

$$Fs = \frac{\sum\left(\left(c'\beta\cos\alpha' + \left(N - u\beta\right)\tan\phi'\cos\alpha'\right)\right.}{\sum N\sin\alpha' - \sum D\cos\omega} \tag{2-8}$$

where *F is Fm* when *N* is substituted into equation (2-7) and *F* is *Fs* when *N* is substituted into equation (2-8). The relationship between the interslice normal force (*E*) and the interslice (*X*) were both considered and the interslice function was derived from a half-sine function.

The soil-water pressure generated from the calibrated SEEP/W model was used as input into SLOPE/W. SLOPE/W was then run using the soil-water pressure at chosen time steps to determine the effect of the changes on the stability of the slip surface. The

auto-search option was chosen for defining possible tension cracks and the potential slip surface. In this method, SLOPE/W generated at least 1000 trial slip surfaces to find the most probable slip surface based on the problem's geometry by identifying the most probable entry and exit areas of the slip surface. This method can result in unrealistic slip outputs so a comparison of the generated slip surface with the actual appearance of the collapsed bank is necessary. One limitation of this version of SLOPE/W is that it only considered pore water pressure effects and not seepage gradient forces when calculating *Fs*.

2.3.3 Quantification of Soil Parameters

Falling head tests quantified K_{sat} values for each density used in seepage experiments (McWhorter and Sunada, 1977). Tests were conducted using a total soil volume of 189 cm^3 packed in four lifts to achieve the desired bulk density. Soil was allowed to saturate from the bottom to the top until water flowed out of the hose at the top of the soil column to indicate saturation. At least eight points were recorded for each test. Following ASTM Standards (D3080-98), laboratory direct shear tests were used to obtain cohesion and angle of internal friction for each density tested.

2.4 Results and Discussion

2.4.1 Soil Physical, Hydraulic, and Geotechnical Characterization

Soil hydraulic and geotechnical properties are listed in Tables 2-1 to 2-4 for both SL1 and SL2 along with a comparison to the soils used by Chu-Agor et al. (2008a). The two sandy loam soils differ significantly in clay content, with SL2 containing more than

twice the clay content of SL1 (Table 2-1). Measured saturated hydraulic conductivity (Table 2-3) of SL1 at the highest density tested (1.7 Mg m^{-3}) was more than an order of magnitude greater than the highest density tested for SL2 (1.60 Mg m^{-3}). Estimated van Genuchten parameters for the two soils were not as contrasting with the greatest difference being the highest density of SL1 and the lowest density of SL2 (Table 2-2). The van Genuchten parameter α is approximately the inverse of the air entry suction value and parameters *n* and *m* are dimensionless curve shape parameters. Values measured for effective cohesion (*c*') for SL1 at a density of 1.60 Mg m^{-3} were almost three times greater than the same soil at a density of 1.45 Mg m^{-3} (Table 2-4).

Table 2-1. Particle size distribution for the two soils used in the soil block experiments and the two soils used by Chu-Agor et al. (2008a).

Soil Texture	% Sand	% Silt	% Clay
Sand (Chu-Agor et al., 2008a)	99	1	0
Loamy Sand (Chu-Agor et al., 2008a)	85	13	2
SL1	66	28	6
SL2	72	13	15

Table 2-2. Soil water retention curves estimated using RETC for the two sandy loam soils.

Soil Type	Bulk density (Mg m^{-3})	θ_r (m^3 m^{-3})	θ_s (m^3 m^{-3})	α (m^{-1})	n	m
SL1	1.70	0.032	0.32	5.0	1.37	1.00
	1.60	0.033	0.34	4.2	1.42	1.00
	1.45	0.036	0.38	3.4	1.46	1.00
	1.30	0.037	0.41	2.8	1.45	1.00
SL2	1.60	0.051	0.51	3.2	1.43	1.00
	1.50	0.055	0.55	2.9	1.49	1.00
Clay	-	-	0.44	1.0	2.00	1.00

Table 2-3. Saturated hydraulic conductivity (K_{sat}) measured using falling head test for varying bulk densities of the two sandy loam soils. Properties of the two sandy loam soils investigated in this research are compared to previous seepage erosion study sand and loamy sand soils used by Chu-Agor et al. (2008a).

Soil Type	Bulk density ($Mg\ m^{-3}$)	Saturated hydraulic conductivity, K_{sat} ($m\ s^{-1}$)
SL1	1.70	1.05×10^{-6}
	1.60	2.34×10^{-6}
	1.45	7.01×10^{-6}
	1.30	9.35×10^{-6}
SL2	1.60	9.35×10^{-8}
	1.50	5.84×10^{-7}
Clay	-	7.34×10^{-9}
Sand	1.60	7.70×10^{-5}
(Chu-Agor et al., 2008a)	1.45	1.76×10^{-5}
	1.30	2.84×10^{-5}
Loamy Sand	1.70	6.00×10^{-6}
(Chu-Agor et al., 2008a)	1.60	1.20×10^{-5}
	1.50	3.40×10^{-6}

Table 2-4. Geotechnical properties of the SL1 measured using laboratory direct shear stress for each density. Properties of the SL1 investigated in this research are compared to previous seepage erosion study sand and loamy sand soils used by Chu-Agor et al. (2008a).

Soil Type	Bulk density ($Mg\ m^{-3}$)	Effective cohesion, c' (kPa)	Internal Angle of Friction, φ' (degrees)
SL1	1.60	11.85	31.6
	1.45	4.22	28.4
Sand	1.60	3.4	40.6
(Chu-Agor et al., 2008a)	1.45	2.0	38.4
	1.30	0.5	26.5
Loamy Sand	1.70	7.4	41.9
(Chu-Agor et al., 2008a)	1.60	4.9	39.1
	1.50	2.5	36.2

2.4.2 Seepage Mechanisms: Erosion and Undercutting versus Tension/"Pop-Out" Failures

Supporting previous observations by Chu-Agor et al. (2008a), bulk density was the controlling factor for the seepage failure mechanism observed in both soils (SL1 and SL2) because of its control on the geotechnical strength of the soil material. Banks collapsed due to seepage either by: (1) tension or "pop-out" failures when the force of the seepage was greater than the resistance of the soil that further decreased as a result of reduced shear strength from increased soil pore-water pressure, and (2) undercutting when seepage force gradient was less than the initial resisting force of the soil block with eventual bank collapse due to the combine forces from seepage and the buildup of pore-water pressure (Chu-Agor et al., 2008a).

Comparing hydraulic and stability parameters to less cohesive soils used by Chu-Agor et al. (2008a) in Tables 2-3 and 2-4 illustrate the range of values tested for each soil. Chu-Agor et al. (2008a) found an increasing trend in the density dependent demarcation point between tension or "pop-out" failures. This increasing trend was observed again with the more cohesive soils, although the demarcation point was approximately equivalent for the two sandy loam soils with varying clay content.

Shapes of the undercuts were unique compared to those observed in less cohesive soils as shown in Figure 2-4. In the sand and loamy sand soils, undercutting shapes were more focused at the center of the soil box with particle entrainment that resulted in less wide and deeper undercuts. This undercutting shape was hypothesized to be due to the converging groundwater flow pathways as water flowed through the high conductivity

soils to the undercut representing the pathway of least resistance. However, undercuts in SL1 and SL2 were much wider and typically extended the entire distance across the face of the soil box. Also, the undercutting process typically occurred as a set of smaller mass failures as the soil became saturated and eventually destabilized the bank to the point of one much larger mass failure. As expected, times to failure were significantly greater in the more cohesive soils. These are shown in Table 2-5, which also illustrates the significant difference in times to failure from sand at 1.45 Mg m^{-3} and 0.15 m head (360 s) to SL1 with the same conditions (7800 s).

Table 2-5. Times to failure for both sandy loam soils at each density tested. Failure times are compared to those observed for a sand and loamy sand soil used by Chu-Agor et al. (2008a).

Soil Type	Bulk density (Mg m^{-3})	Constant Head imposed at Box Inlet (m)	Time to Failure (s)
Sand (Chu-Agor et al., 2008a)	1.60	0.25	635, 537
		0.15	723, 732
	1.45	0.25	440, 490
		0.15	384, 346
Loamy Sand (Chu-Agor et al., 2008a)	1.70	0.35	1534
		0.25	3206
		0.15	3262
	1.60	0.35	1350
		0.25	2820
		0.15	3895
SL1	1.70	0.35	53460, 55140
		0.25	-
		0.15	-
	1.60	0.35	26640
		0.25	14820, 24420
		0.15	65700, 75000
	1.45	0.25	2880, 1800
		0.15	5700, 9900
	1.30	0.25	1620, 1740
		0.15	6360, 8040
SL2	1.60	0.25	48660, 72000
	1.50	0.25	43200, 15600

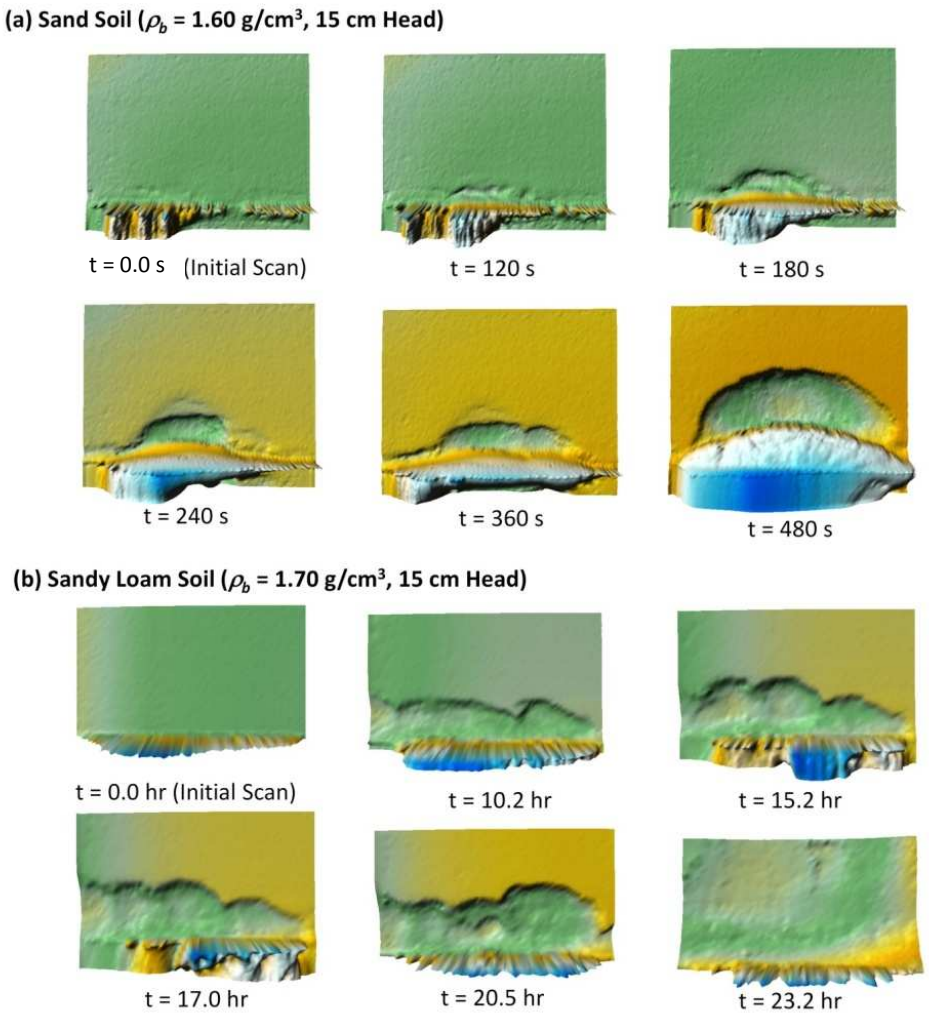

Figure 2-4. Scans showing undercutting for (a) sand (Chu-Agor et al., 2008a) and (b) SL1.

2.4.3 Seepage Modeling: Flow Modeling and Calibration of SEEP/W

Inflow data from a subset of laboratory seepage tests were then used as the basis for calibration of SEEP/W models with the same conditions. Cumulative mass flux at the inlet and outlet were taken from each SEEP/W model run and compared with observed data from the laboratory. Hydraulic conductivity and van Genuchten (1980) parameters were calibrated to match the SEEP/W inflow and outflow to observed laboratory data. These calibrated parameters are shown in Table 2-6. Due to possible discrepancies when

packing soil boxes of this scale, calibrated K_{sat} values were slightly different for the modeled soil profiles at the same density but different heads. Table 2-7 shows the root mean square error (RMSE) and coefficient of determination (R^2) values for each calibration.

Table 2-6. Calibrated soil water retention curves and hydraulic conductivities for SL1 at bulk densities 1.60 and 1.45 Mg m^{-3}.

Soil Type	Head (m)	Bulk Density (Mg m^{-3})	K_{sat} (m/s)	α (m^{-1})	n	m
SL1	0.25	1.60	7.34E-7	5.0	2.5	0.15
	0.15	1.60	9.34E-7	5.0	2.5	0.15
	0.25	1.45	4.00E-6	3.0	2.5	0.2
	0.15	1.45	2.50E-6	3.0	2.0	0.2

Table 2-7. Statistical analysis of laboratory inflow and outflow versus SEEP/W inflow and outflow.

Soil Type	Flow Face	Head (m)	Bulk Density (Mg m^{-3})	n	RMSE	R^2
SL1	Inlet	0.25	1.60	84	4.00E-4	0.98
	Outlet	0.25	1.60	84	1.45E-4	0.97
	Inlet	0.15	1.60	101	6.87E-4	0.96
	Outlet	0.15	1.60	101	9.06E-5	0.96
	Inlet (1)	0.25	1.45	51	1.65E-3	0.98
	Inlet (2)	0.25	1.45	35	7.53E-4	0.96
	Inlet	0.15	1.45	11	4.80E-4	0.89

2.4.4 Stability Modeling: Slope and stability calculations in SLOPE/W

Initially all SLOPE/W models began with a factor of safety ranging from 10 to 25, indicating the resistive forces in the soil were much greater than the driving forces. However, when the head was applied at the inlet and pore-water pressures began to

increase, in most cases the factory of safety decreased immediately. Figure 2-5(a) shows the flow lines and water table from SEEP/W and Figure 2-5(b) shows the corresponding stability calculations in SLOPE/W for an example scenario. Figures 2-6 and 2-7 presents the calculated *Fs* over time for SL1 at a density of 1.60 Mg m^{-3} and heads of 0.15 and 0.25 m. An effective cohesion of 11.9 kPa was calculated from laboratory direct shear tests, utilized in the model, and resulted in a final *Fs* of 9.0 and 8.8 for heads of 0.25 m and 0.15 m respectively. To demonstrate that the model does not predict failure even with lower cohesion values, *c'*= 5.0 and 10.0 kPa were both tested in SLOPE/W. With the lowest value of *c'*=5.0 kPa, the model predicted a final *Fs* of approximately 4.

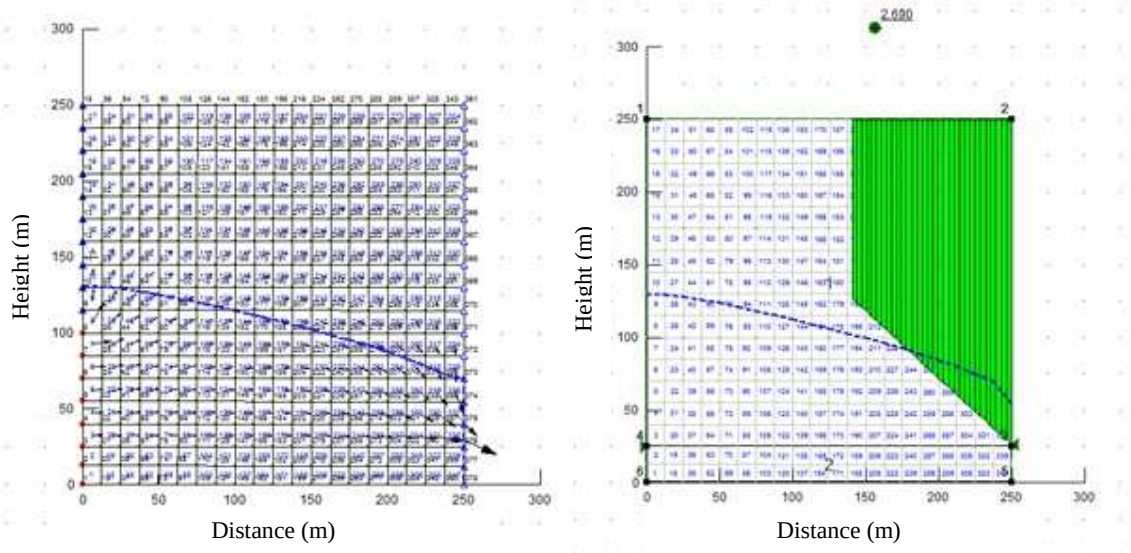

Figure 2-5. GeoSlope (a) SEEP/W flow calibration and (b) SLOPE/W stability analysis with SEEP/W pore water pressures.

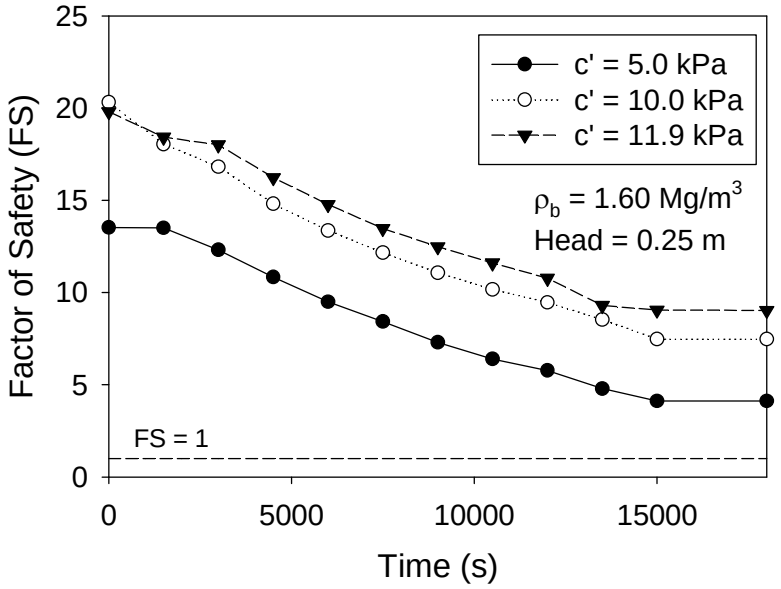

Figure 2-6. Factor of Safety over time for SL1 at 1.60 Mg m^{-3} with 0.25 m of head with geotechnical parameter *c'* ranging from 5.0 to 11.9 kPa.

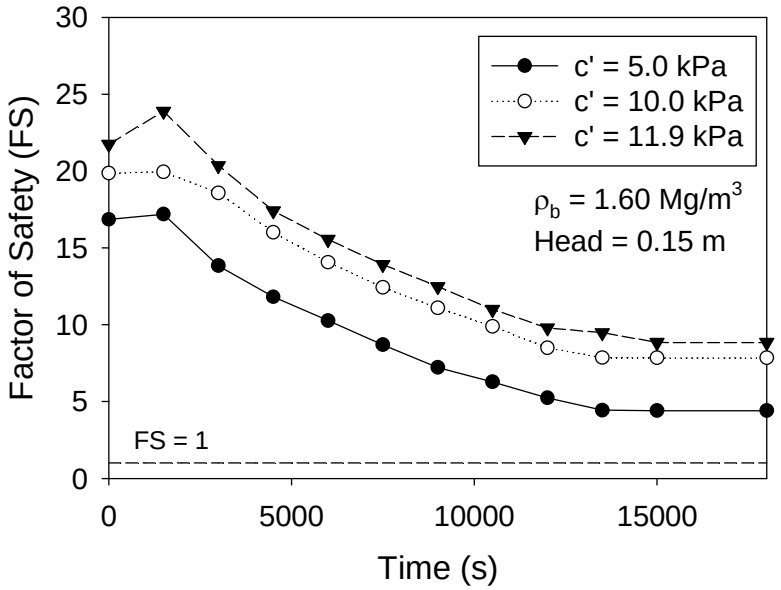

Figure 2-7. Factor of Safety over time for SL1 at 1.60 Mg m^{-3} with 0.15 m of head with geotechnical parameter *c'* ranging from 5.0 to 11.9 kPa.

SLOPE/W *Fs* calculations for SL1 with a density of 1.45 Mg m^{-3} at heads of 0.15 and 0.25 m are shown in Figures 2-8 and 2-9. An effective cohesion of 4.2 kPa was calculated from laboratory direct shear tests, utilized in the model, and resulted in a final *Fs* of 4.0 and 3.9 for heads of 0.25 m and 0.15 m respectively. Again, the model still does not predict failure even when underestimating *c'*.

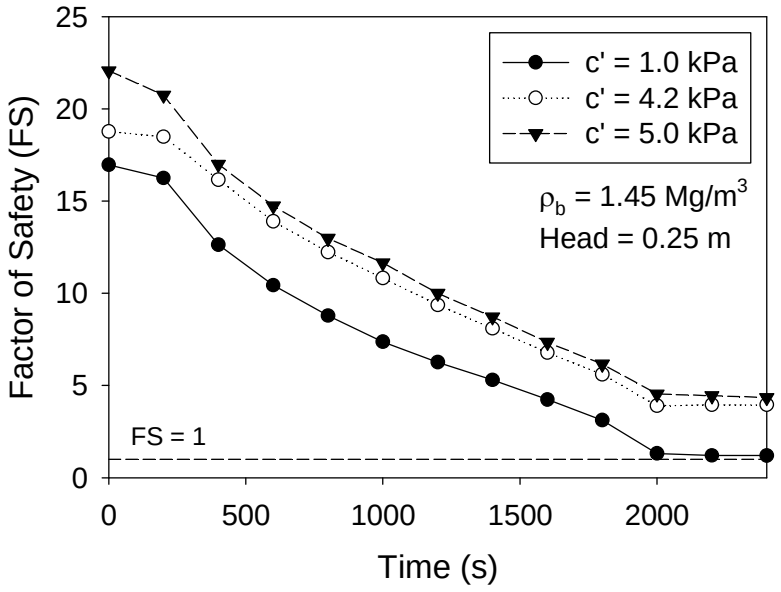

Figure 2-8. Factor of Safety over time for SL1 at 1.45 Mg m^{-3} with 0.25 m of head with geotechnical parameter *c'* ranging from 1.0 to 5.0 kPa.

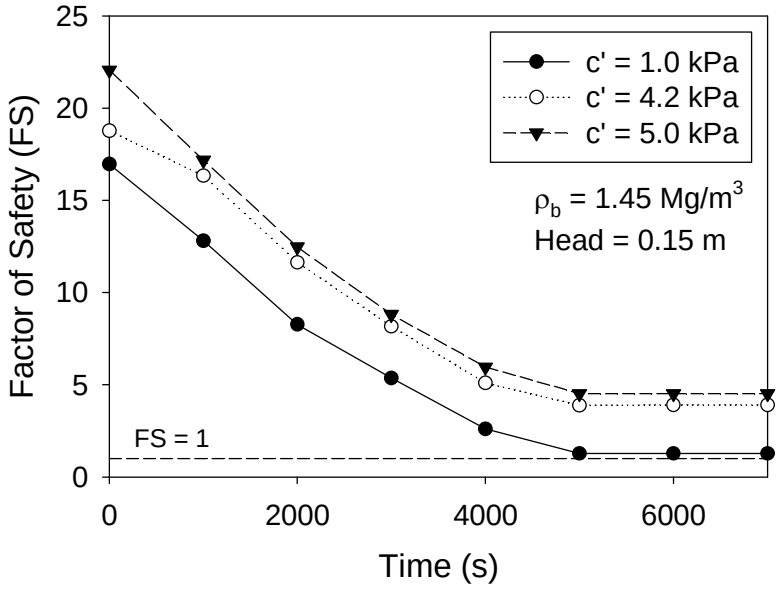

Figure 2-9. Factor of Safety over time for SL1 at 1.45 Mg m^{-3} with 0.15 m of head with geotechnical parameter *c'* ranging from 1.0 to 5.0 kPa.

2.5 Summary and Conclusions

Seepage erosion in hillslopes, gullies and streambanks results in tension ("pop-out") failure when seepage forces are greater than soil resistance and shear strength is reduced from an increase in soil pore-water pressure or particle entrainment and mobilization resulting in undercutting and eventual mass-failure. Previous research indicated a demarcation point between these two failure mechanisms that was determined to be density dependent for sand and loamy sand soils. In sands, the demarcation point was at a density of 1.3 Mg m^{-3} and in loamy sands at 1.5 Mg m^{-3}. This increasing trend was observed with more cohesive soils although the demarcation point (1.60 Mg m^{-3}) was approximately equivalent for the two sandy loam soils with varying clay content.

Times to failure were significantly longer for SL1 and SL2 than in the less cohesive soils tested by Chu-Agor et al. (2008a). Failure times for the more cohesive soils were three to ten times greater under similar conditions. Higher failure times allowed for a greater volume of water to flow into the soil, leading to a greater failure volume for more cohesive soils due to the added weight and volume of saturated soil. Undercutting shapes in both sand and loamy sand soils were more focused at the center of the soil box with particle entrainment that resulted in less wide and deeper undercuts. However, undercutting in sandy loam soils was much wider and typically extended the entire distance across the face of the soil box. Also, the undercutting process typically occurred as a set of smaller mass failures as the soil became saturated and eventually destabilized the bank to the point of one much larger mass failure.

A subset of laboratory experiments was simulated using SEEP/W and SLOPE/W to quantify the factor of safety over time. Calibrations were performed in SEEP/W to match flows observed in the laboratory experiments. SLOPE/W used pore-water pressures from SEEP/W to calculate factors of safety for the slip surface. While a failure was observed in the laboratory under the modeled conditions, SLOPE/W was unsuccessful at predicting a failure and leveled out at a theoretically stable factor of safety even when under estimating the effective cohesion. SLOPE/W only considered pore-water pressures in its stability analysis; seepage gradient forces were neglected leading to an over estimation of the stability of these slopes.

CHAPTER III

LABORATORY SOIL PIPING AND INTERNAL EROSION EXPERIMENTS: EVALUATION OF A DETERMINISTIC SOIL PIPING MODEL

3.1 Abstract

Soil piping has been attributed as a potential mechanism of instability for embankments, hillslopes, dams, and streambanks. In fact, deterministic models have been proposed to predict soil piping and internal erosion. However, limited research has been conducted under controlled conditions to evaluate these models. The objective of this study was to utilize a constant-head soil box (0.50 m long x 0.50 m wide x 0.20 m tall) to conduct soil pipe experiments and derive flow and internal erosion data for two soils packed at uniform bulk densities but different initial moisture contents. Soils included a clay loam from Dry Creek in northern Mississippi and a sandy loam from Cow Creek in northern Oklahoma. Initial gravimetric moisture contents were 10, 12 and 14% for Dry Creek soil and 8, 12, and 14% for Cow Creek soil. A 1-cm diameter rod was placed horizontally along the length of the soil bed during packing and carefully removed after packing to create a continuous soil pipe. A constant head was maintained at the inflow end of the soil pipe. Flow rates and sediment concentrations were measured from the pipe outlet. Submerged jet erosion tests (JETs) were conducted to derive erodibility

parameters for repacked samples at the same moisture contents as the box experiments. Flow rates from the box experiments were used to calibrate the deterministic model based on erodibility parameters. The influence of the initial moisture content of the packed soil was apparent, with some pipes (8% moisture content) expanding so fast that limited data was able to be collected during the experiment. The deterministic model was able to estimate equivalent flow rates to those observed in the experiments, but had difficulty matching observed sediment concentrations when the pipes rapidly expanded by internal erosion. The JETs predicted similar erodibility coefficients compared to the deterministic model for the more erodible cases (8 and 12% moisture content), but not for the less erodible cases (14% moisture content). Improved models are needed that better define the changing cross-section of a soil pipe during both supply-limited and transport-limited internal erosion.

Keywords: Internal Erosion, Jet Erosion Test, Piping, Soil Erodibility

3.2 Introduction

Subsurface flow can be a destabilizing force for hillslopes, streambanks, gullies, and embankments by several mechanisms including: (1) seepage leading to an increase in the pore-water pressure which reduces the apparent cohesion of the soil and increases the weight of the soil; (2) seepage gradient forces causing the soil slope to collapse or fail; and (3) seepage flow resulting in particle mobilization and seepage undercutting (Fox and Wilson, 2010). The role of seepage in increasing pore-water pressure and decreasing the soil strength has been documented by a number of researchers (Fredlund and Rahardjo, 1999; Darby et al., 2007). Seepage erosion experiments have been performed by multiple

authors in the last few years (Chu-Agor et al., 2008a; Fox and Wilson, 2010). These experiments have typically focused on particle mobilization and undercutting.

Another mechanism by which subsurface flow can destabilize soils is through soil piping, or flow through an open macropore, i.e. soil pipe, leading to internal erosion of the soil pipe walls which can result in streambank failure, gullies, and embankment failure (Fox and Wilson, 2010). The pipeflow, particle detachment, and sediment transport processes involved are complex. Internal erosion of a soil pipe is typically described by the classic excess shear stress equation (Fox and Wilson, 2010):

$$q_s = k_d(\tau - \tau_c)^b \tag{3-1}$$

where q_s is the sediment transport rate (kg m^{-2} s^{-1}), k_d is the erodibility coefficient (s m^{-1}), τ is the hydraulic shear stress on soil particles, τ_c is the critical shear stress (Pa), and b is an empirical coefficient commonly assumed to be unity. This equation was developed for and typically applied to overland flow which involves a two-dimensional planar surface. For a water-filled soil pipe, these forces act on the two-dimensional radial surface of the pipe and along its length, thereby enlarging the pipe circumference as a function of length along the soil pipe. For conditions in which a soil pipe extends through a reservoir's embankment, as the pipe enlarges the "infinite" head of the reservoir can maintain water-filled conditions (Bonelli et al., 2006). Flow rates increase as the pipe enlarges, thereby, providing a positive feedback mechanism that result in more rapid internal erosion. Soil pipe enlargement progresses rapidly to the point that the soil above can no longer be supported and the soil pipe collapses resulting in an embankment breach or mature gully formation. Another important pipeflow erosion mechanism involves pipe clogging as a result of sediment transport limitations. When internal erosion exceeds the

sediment transport capacity, pipe clogging can occur which has been postulated (Pierson, 1983; Uchida et al. 2001) to result in pressure build ups that can cause sudden mass failures of hillslopes (e.g., landslides and debris flows). In laboratory soil pipeflow experiments, Wilson (2009, 2011) noted that clogging resulted in surges in pipeflow. Such turbulent flow conditions resulted in high sediment concentrations and rapid expansion of the pipe diameter. Numerical simulations of these experiments (Wilson and Fox, 2013) indicated that the clogging, even for periods as short as 0.1 s, produced almost instantaneous pressure buildups within the soil pipes.

In order to model turbulent pipeflow and internal erosion, previous research has used an analytical solution developed by Bonelli et al. (2006). They used two-phase flow equations (water-particles mixture and the particles) with interface erosion for modeling flow and erosion in a soil pipe. The soil was assumed homogeneous, rigid, and neglected hydraulic transfer between the matrix and pipe domains. The model assumed axisymetrical flow with large Reynolds number and uniform pressure across each pipe section. Bonelli et al. (2006) assumed a linear relationship (b=1) in the excess shear stress equation. The radius was assumed axially uniform and the concentration was uniform in a section. As erosion occurs, a mass flux crosses the time-dependent interface, and therefore, the current interface undergoes a transition from solid-like to fluid-like behavior (Bonelli et al., 2006). The proposed model was shown to conform to experimental data from Hole Erosion Tests (HET) on nine different soils. The HET measures changes in flow rate with time to back-calculate changes in the pipe diameter and thus the internal erosion. The HET allows calculation of the soil erodibility and

critical shear stress. They used the negative log of the soil erodibility as an Erosion Rate Index to characterize the internal erosion of materials (Wan and Fell, 2004).

For overland flow erosion of cohesive soils, Hanson (1990) developed the jet erosion test (JETs) to estimate the erodibility coefficient, k_d, and critical shear stress, τ_c, of soils. In order to create a measurable scour hole from which k_d and τ_c can be calculated, the JET directs a jet of water towards the soil. Periodically, the jet is blocked by a deflector plate and a point gauge is used to measure the depth of the scour hole. Measurements are taken until the scour depth reaches an equilibrium depth. Using diffusion principles, analytical solutions are used to derive k_d and τ_c from the observed scour depth versus applied shear stress data (Al-Madhhachi et al., 2012a). Hanson and Hunt (2007) used a laboratory version of the original JET device to estimate the soil erodibility and compared the results with field embankment erosion tests to study the internal erosion on breach widening due to seepage piping. Similar values of estimated k_d were observed between laboratory original JET device and field embankment erosion tests.

A new miniature version of JET device ("mini" JET), which was utilized in this study, was recently developed. Al-Madhhachi et al. (2012a) verified the results of the "mini" JET to predict the soil erodibility with the larger original JET device under controlled laboratory settings. Both original and "mini" JET devices have been shown to provide equivalent results to flume experiments in predicting the soil erodibility (Al-Madhhachi et al., 2012b).

Wilson et al. (2012) reviewed the experimental and numerical work conducted on pipeflow and resulting internal erosion. They identified the need for future studies that evaluate pipeflow and internal erosion models: "…advances are needed in the ability to model the preferential flow, sediment detachment, internal mass failures, and sediment transport processes associated with internal erosion of soil pipes." The objectives of this research were to (i) conduct laboratory soil piping experiments on two contrasting soils packed at uniform bulk densities but at different initial moisture contents, (ii) conduct "mini" JETs on similarly packed soils in standard molds, and (iii) use these data to evaluate the Bonelli et al. (2006) model.

3.3 Methods and Materials

3.3.1 Laboratory Experiments

Laboratory soil pipe experiments were conducted on both Dry Creek and Cow Creek streambank soils. Dry Creek (33.7485N, 89.1725W), located in Chickasaw County, Mississippi, is a tributary to Little Topashaw Creek (LTC), a 37 km^2 experimental subwatershed of the Topashaw Canal CEAP watershed in Mississippi (Wilson et al., 2007). The creek flows through alluvial plains under cultivation that are surrounded by forested areas. Wilson et al. (2007) identified excess sediment as the main water quality issue within this watershed. Dry Creek is a deeply incised stream with near 90^o banks consisting of Urbo silty clay loam soils (fine, mixed active, acid, thermic Vertic Epiaquepts), Rhoades et al. (2007). Midgley et al. (2012a) reported the site having a clay loam (37% sand, 34% silt and 29% clay) surface soil with a bulk density near 1.6 Mg m^{-3}. Located in Payne County, Oklahoma (36.1213N, 97.0998W), Cow Creek is

currently deepening and widening with the formation of associated side-gullies. Streambanks consist of a Pulaski fine sandy loam (coarse-loamy, mixed, superactive, nonacid, thermic Udic Ustifluvents) with a sandy loam surface (55% sand, 19% silt, and 26% clay). Midgley et al. (2012b) conducted field experiments on soil piping at these sites, but focused more on the influence of soil pipe clogging on the resulting pore-water pressures in the field.

Experiments were conducted using a Plexiglas box of dimensions 50 cm wide by 50 cm long and 50 cm tall (fig. 3-1). Soil was packed into the box with dimensions 50 cm wide, 50 cm deep, and 20 cm tall. Cow Creek soil was packed at a bulk density of 1.5 Mg m^{-3} and Dry Creek soil was packed at a bulk density of 1.6 Mg m^{-3}, which mimicked values in the field. Experiments were run for each streambank soil packed to the specified bulk densities at various initial moisture contents by weight (Table 3-1).

Previous research indicated a relationship between moisture content at packing and the erodibility properties of soil (Hanson and Hunt, 2007; Regazzoni et al., 2008; Al-Madhhachi et al., 2012a): the k_d of soil was dependent on the water content at different compaction energies. For compaction at the same energy, Lambe (1962) surmised that the compaction effects on soil structure at different water contents was related to the arrangement of soil particles and the electromagnetic forces between neighboring particles. At low water contents, the electrical repulsive forces between particles are smaller than the attractive forces. This results in a net attraction between the particles; therefore, the particles tend to flocculate in a disorderly array (Lambe, 1962). A more orderly array of particles can be observed as water content increases until the soil reaches its optimum water content due to an increase in the repulsive forces between the particles,

resulting in the maximum bulk density. Beyond the optimum water content, a parallel arrangement between soil particles leads to a decrease in bulk density (Lambe, 1962).

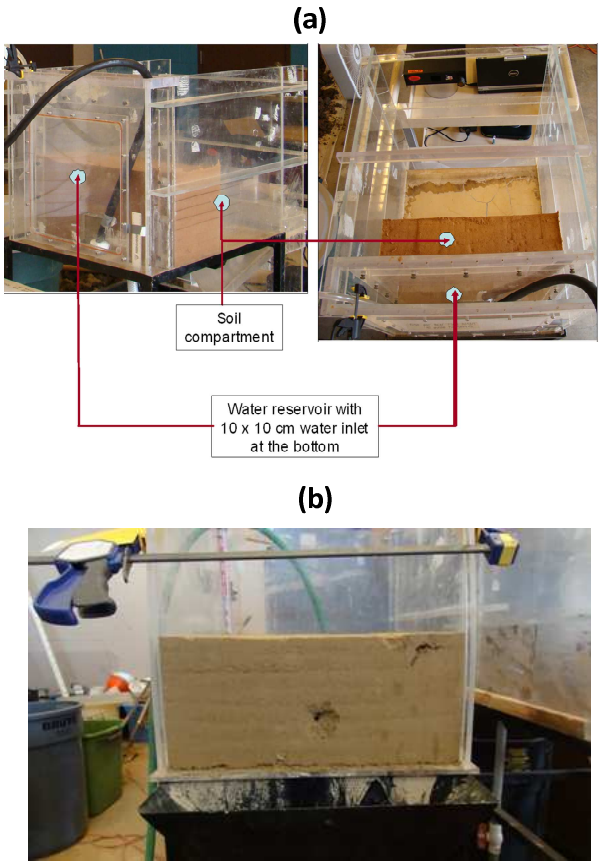

Figure 3-1. Experimental set-up for the soil piping experiments. (a) Side view and top view of the soil box not completely packed. (b) Front-view of Dry Creek soil in completely packed soil box.

A 1-cm diameter rod was horizontally placed approximately 5 cm above the base of the soil box, extending the full length of the soil bed during packing, and removed once the soil was completely packed to create a continuous soil pipe with approximately no slope. A constant-head was imposed on the soil pipe at heads depending on the experimental conditions (Table 3-1). For most experiments, it was difficult to maintain a

specific constant head due to internal erosion enlarging the soil pipe beyond the capacity of the setup to maintain the desired head. For such instances, the head was estimated based on average head observed during these periods. Flow from the soil pipe was captured in a flume at the end of the soil box and collected in a container (18.9 L). A weighing scale (A&D HW-60KGL Platform Scale) was placed at the outlet to monitor outflow from the pipe with a resolution of 5 g. A computer recorded the values from the scale every 5 s. The container was switched periodically throughout the experiment in order to collect sediment samples over time for quantifying sediment concentrations. A sediment sample was acquired after manually agitating the bucket's contents to evenly distribute the sediment.

Table 3-1. Experimental pipeflow conditions simulated in the laboratory soil boxes with constant initial radius of the pipe, Ro = 1 cm, and length of the soil pipe, L = 0.5 m.

Streambank	Soil Texture			Experiment Number	Bulk Density, ρ_b	Moisture Content at Packing, MC	Constant Water Head, H_{in}[a]	Maximum Pipeflow Rate, Q
	% Sand	% Silt	% Clay		(Mg/m^3)	(%)	(m)	(m^3/s)
Dry Creek	37	34	29	DC 1	1.6	10	NA[b]	4.6×10^{-4}
				DC 3	1.6	12	0.02	1.3×10^{-4}
				DC 2	1.6	14	0.04	3.0×10^{-5}
Cow Creek	55	19	26	CC 1	1.5	12	0.08	2.2×10^{-4}
				CC 3	1.5	8	0.07	1.7×10^{-4}
				CC 7	1.5	14	0.08	2.1×10^{-5}

[a] Estimated average head from videos of the laboratory experiments, as water level could not be maintained at initial starting head of 15 cm after pipe expansion.
[b] In this experiment, the pipe eroded quickly and constant head could not be maintained on the soil.

At the end of three experiments in which the soil pipe stayed open throughout the experiment, expandable foam was shot into the soil pipe from the face of the soil bed.

This expandable foam was allowed to dry for 24 hr and then the foam cast was extracted from the bed. Calipers were used to measure the dimensions of the soil pipe along its length.

3.3.2 Laboratory "Mini" JETs

Duplicate "mini" JETs were conducted on repacked soils at the same moisture contents as shown in Table 3-1. The procedure for using the "mini"-JET followed Al-Madhhachi et al. (2012a), as shown in Figure 3-2. For the laboratory JETs, soils were air dried and then sieved. To achieve the desired water content, the soils were mixed with different quantities of water and left for 24 hr in a closed bucket to allow for moisture equilibrium. Then, the samples were compacted in three equal lifts in the standard mold to the target bulk density. The device was then placed on the mold and locked in, sealing the device to the base. The submergence tank was filled with water and testing initiated. Periodically, the jet was blocked by a deflector plate and an installed point gauge was used to measure the depth of the scour hole (fig. 3-2). Measurements were taken until the scour depth reached equilibrium. Scour depth versus time data were analyzed following Al-Madhhachi et al. (2012a) to estimate k_d and τ_c.

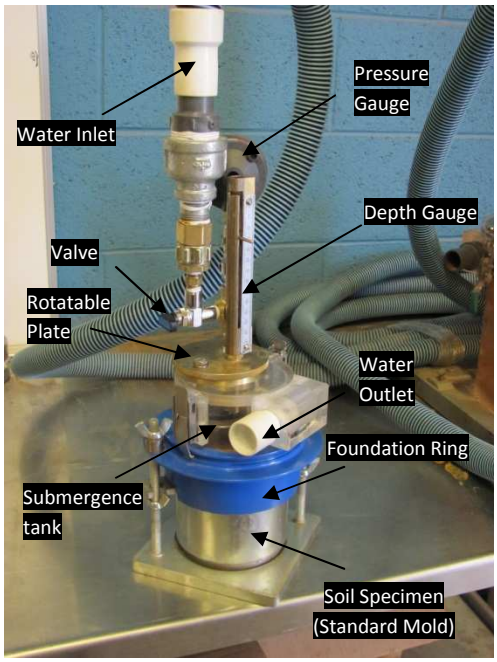

Figure 3-2. Laboratory "mini" JET device (Al-Madhhachi et al., 2012a).

3.3.3 Pipeflow Modeling

The flow rate and sediment concentration data from each experiment were used to evaluate the Bonelli et al. (2006) pipeflow model. Based on a soil pipe of length L and initial radius R_o, the model predicted the radius of the pipe, $R(t)$, as a function of time, t, mean longitudinal velocity, $V(t)$, and the corresponding flow rate, $Q(t)$:

$$\frac{R(t)}{R_o} = 1 + \left(1 - \frac{\tau_c}{P_{fl}}\right)\left[\exp\left(\frac{t}{t_{er}}\right) - 1\right] \tag{3-2a}$$

$$\frac{V(t)}{V_{fl}} = \sqrt{\frac{R(t)}{R_o}} \tag{3-2b}$$

$$Q(t) = Q_{fl}\left(\frac{R(t)}{R_o}\right)^{5/2} \tag{3-2c}$$

where t_{er} is a characteristic erosion time (s) which depends on k_d, L, and the density of the sediment, ρ_g, as shown in equation (3-3), P_{fl} is the assumed constant hydraulic stress (Pa) as a function of the input (p_{in}) and output pressures (p_{out}) as shown in equation (3-4), Q_{fl} is the initial entrance flow ($m^3\ s^{-1}$), and V_{fl} is a reference velocity ($m\ s^{-1}$) as shown in equation (3-5):

$$t_{er} = \frac{2L\rho_g}{k_d(p_{in} - p_{out})} \tag{3-3}$$

$$P_{fl} = \frac{R_o(p_{in} - p_{out})}{2L} \tag{3-4}$$

$$V_{fl} = \frac{Q_{fl}}{\pi R_o^{\ 2}} \tag{3-5}$$

From these equations, it is possible to derive an equation for the shear stress at the interface, τ:

$$\tau = P_{fl}\frac{R(t)}{R_o} \tag{3-6}$$

Using equations (3-1) through (3-6), the erosion rate, q_s, can then be combined with the predicted $Q(t)$ to estimate the eroded concentration, $C(t)$:

$$C(t) = \frac{q_s(t)A}{Q(t)} = \frac{2\pi R(t) L q_s(t)}{Q(t)} \tag{3-7}$$

An alternative but equivalent form can be derived from the predicted $R(t)$ during a specified time interval, Δt:

$$C(t) = \frac{\frac{\pi\left(R(t)^2 - R_o^{\ 2}\right)L\rho_g}{\Delta t}}{Q(t)} \tag{3-8}$$

The flow rates and sediment concentration data from each experiment was modeled by fitting k_d and τ_c based on minimizing the sum of squared errors between observed and predicted flow rates during the experimental period. The quality of the model fit was assessed based on the root mean square error and a normalized objective function (Fox et al., 2006):

$$RMSE = \sqrt{\frac{\sum_{i=1}^{n}(X_i - Y_i)^2}{n}} \tag{3-9}$$

$$NOF = \frac{RMSE}{X_a} \tag{3-10}$$

where X_i and Y_i are the observed and predicted values, respectively; X_a is the mean of observed values; and n is the number of observations. In general, 1%, 10%, and 50% deviations from the observed values result in NOF values of 0.01, 0.10, and 0.50, respectively.

3.4 Results and Discussion

Three Dry Creek experiments were run at 10%, 12% and 14% gravimetric moisture contents (Table 3-1). The 10% moisture content packing eroded so quickly within the 6.5 minute duration of the experiment that the initial head could not be maintained on the soil. The flow rate quickly increased and then stabilized throughout the remainder of the experiment as the head was adjusted, resembling an asymptotic function and contradicting the theoretical behavior of the pipeflow model. This experiment was not fit with the Bonelli et al. (2006) model since a constant flow rate as opposed to a constant head was achieved for the experiment. Sediment concentrations were fairly constant throughout the duration of the experiment at approximately 30 g/L.

The 12% moisture content eroded at a similar rate to the 10% moisture content experiment. Average flow rates were similar but this experiment did more closely resemble a constant head experiment with an average head of 2 cm and increasing flow rates as internal erosion increased the pipe radius (fig. 3-3). The test duration was approximately 5.5 minutes and average sediment concentrations were approximately 74 g/L. Sediment concentrations decreased during the duration of the experiment.

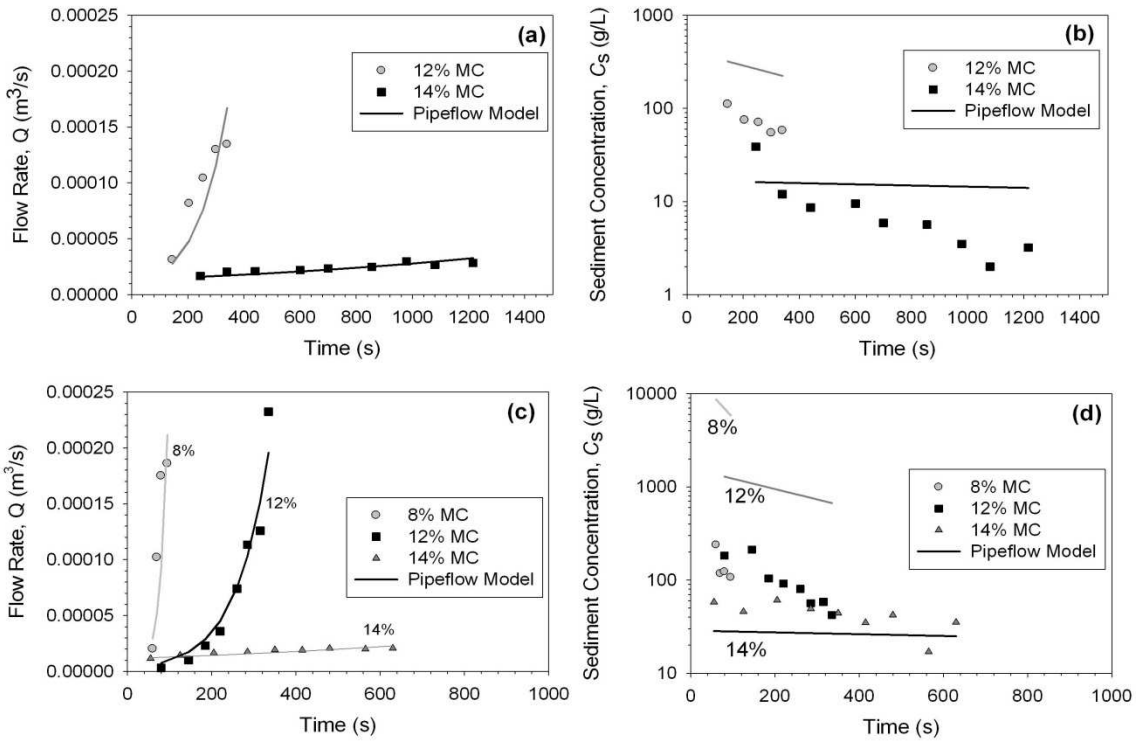

Figure 3-3. Calibrated versus observed pipe flow rate, *Q*, data using the Bonelli pipeflow model at (a) Dry Creek and (c) Cow Creek and the predicted versus observed sediment concentrations, C_s, at (b) Dry Creek and (d) Cow Creek.

The final Dry Creek experiment packed at 14% moisture content had an approximately 4 cm head imposed on the soil pipe. This condition resulted in a lower maximum flow rate, most likely because the pipe failed to expand as much as earlier experiments. Sediment concentrations were approximately 10 g/L (fig. 3-3). Again, sediment concentrations decreased during the duration of the experiment. The soil pipe in this experiment remained open at the end of the experiment. Final dimensions were only slightly larger than the initial 1.0 cm diameter with widths and heights that averaged 1.1 and 1.0 cm, respectively, based on five sampling locations along the pipe length. Note that the sampling locations did not include the entry and exit points of the eroded pipe as

these locations deviated significantly from the assumed constant radius pipe assumption as a result of the localized excess shear stresses (fig. 3-4).

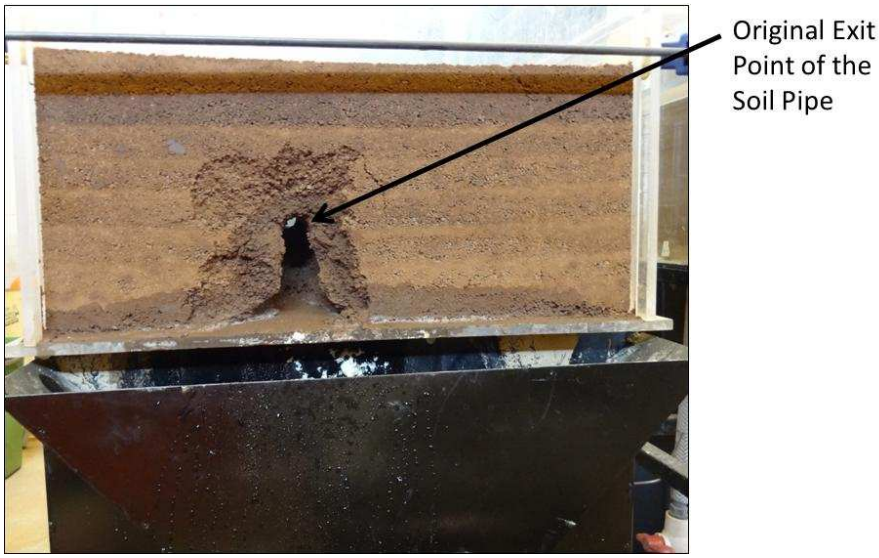

Figure 3-4. Example illustration of the eroded soil pipe at the end of the 8% Cow Creek soil experiment. Picture is from the front face of the box (i.e., exit point of the soil pipe).

Three Cow Creek experiments were performed with soils packed at a uniform bulk density but prepared at 8, 12, and 14% gravimetric moisture contents. The 8% moisture content soil quickly eroded and the experiment only lasted 1.5 minutes due to the imposed 7.0 cm hydraulic head. Observed sediment concentrations were approximately 150 g/L and again decreased in the four samples obtained within the limited time period of the experiment. The pipe remained open during this short duration experiment with average widths and heights of 2.9 and 3.2 cm, respectively, based on measurements at five locations along the pipe length, again neglecting the entry and exit locations (fig. 3-4).

The experiment on the 12% moisture content utilized a slightly higher hydraulic head compared to the previous experiment (7.5 cm) but eroded much slower and the duration was approximately 5.5 minutes. Sediment concentrations were approximately 100 g/L on average and decreased over time once again. The pipe remained open with average widths and heights much greater than the initial dimensions (3.1 and 3.1 cm, respectively, based on measurements at three locations along the pipe length).

A similar head (7.5 cm) was maintained on the soil bed experiment with the 14% gravimetric moisture content, but this experiment produced the smallest flow rates of the Cow Creek experiments, again due to smaller internal erosion limiting the expansion of the pipe radius. This experiment resulted in the lowest average sediment concentrations at approximately 40 g/L for this soil. Experimental durations were over 10 minutes.

The Bonelli et al. (2006) model was able to estimate equivalent flow rates to those observed in pipeflow experiments for both soil types with NOF typically less than 0.20 (Table 3-2 and fig. 3-3). Sensitivity to k_d was much greater than τ_c in the model predictions. In fact, any τ_c less than 0.1 Pa provided equivalent results in the Bonelli et al. (2006) model. Note also that the model matched sediment concentrations for the Dry Creek experiments better than sediment concentrations for the Cow Creek experiments (fig. 3-3). For the Cow Creek experiments, the model performed well for the case with a low flow rate and low internal erosion. However, when the pipe eroded rapidly, the model tended to over predict sediment concentrations. It is hypothesized that in those cases that the pipe was eroding so fast that a transport-limited condition was created (i.e., particle and/or aggregate detachment exceeded the sediment transport capacity of the pipe). In all cases it was observed that model assumptions regarding the geometric

structure of the pipe, assumed consistent along the pipe length, were violated. It was observed that simple geometries no longer represented cases in which the material quickly eroded and the pipe expanded preferentially at the bottom of the pipe cross-section and at the exit of the soil pipe (fig. 3-4). Therefore, more sophisticated models are needed that better define the changing cross-section of a soil pipe during the internal erosion process. This may require evolving domain numerical simulations. Also, more fundamental sediment transport models may be necessary that are able to account for gradient forces between the soil pipe and matrix domains and supply- or transport-limited conditions.

Table 3-2. Calibrated values of the erodibility coefficient, k_d, and critical shear stress, τ_c, for pipeflow rate data.

Streambank	Moisture Content (%)	Erodibility Coefficient, k_d	Critical Shear Stress, τ_c	Normalized Objective Function, NOF[a]
		(s/m)	(Pa)	
Dry Creek (DC)	12	6.6×10^{-2}	<0.1	0.26
	14	2.0×10^{-3}	<0.1	0.10
Cow Creek (CC)	8	8.7×10^{-2}	<0.1	0.26
	12	1.9×10^{-2}	<0.1	0.40
	14	1.6×10^{-3}	<0.1	0.09

[a] NOF calculated based on observed versus predicted flow rates.

The "mini" JETs predicted similar values of k_d compared to fitting the Bonelli et al. (2006) model to the laboratory flow data (Table 3-3, fig. 3-5) for the more erodible cases. The JET-derived k_d for the less erodible cases (14% moisture content) were typically much greater than from those predicted by the Bonelli et al. (2006) model. Note that the JET-derived k_d were similar to those reported by Midgley et al. (2012b) for JET measurements in the field on undisturbed Cow Creek and Dry Creek streambanks with

greater differences observed in the τ_c: Cow Creek k_d = 1.0 x 10^{-1} s m^{-1} and τ_c < 0.1 Pa and Dry Creek k_d = 2.8 x 10^{-2} s m^{-1} and τ_c = 7.9 Pa. However, the soil pipes in these repacked laboratory experiments were much more erodible than observed in the field when using constant-head trench system for the Dry Creek soil (Midgley et al., 2012b). Observations for the repacked Cow Creek soil were consistent with observations in the field.

Table 3-3. Values of the erodibility coefficient, k_d, and critical shear stress, τ_c, from jet erosion tests (JETs).

Streambank	Soil Texture			Bulk Density, ρ_b	Moisture Content at Packing, MC	Erodibility Coefficient, k_d	Critical Shear Stress, τ_c
	% Sand	% Silt	% Clay	(Mg/m^3)	(%)	(s/m)	(Pa)
Dry Creek	37	34	29	1.6	12	7.1 x 10^{-2}	0.01
				1.6	14	6.1 x 10^{-2}	0.02
Cow Creek	55	19	26	1.5	8	1.1 x 10^{-1}	0.10
				1.5	12	5.2 x 10^{-2}	0.08
				1.5	14	5.1 x 10^{-2}	0.01

3.5 Conclusions

Calibrating the deterministic model to the soil pipe flow rate measurements was possible, but resulted in discrepancies between observed and predicted sediment concentrations for cases with highly erodible soil pipes. Submerged jet erosion tests on repacked soil samples derived similar values of the erodibility parameters only for the more erodible soils. Therefore, the laboratory pipeflow experiments demonstrated that improved deterministic models are needed to better simulate soil piping processes. In many cases, soil pipes erode so quickly that transport-limited conditions can be created, which may potentially lead to pipe clogging and the buildup of pore water pressures that can cause geotechnical failure. Also, model assumptions regarding the geometric

structure of the pipe were violated. It was observed that simple geometries no longer represented cases in which the material quickly eroded and the pipe expanded preferentially at the bottom of the pipe cross-section where shear stresses were higher. Soil piping plays a significant role in a number of geomorphological processes and therefore more research should be devoted to being able to explain and model these observations.

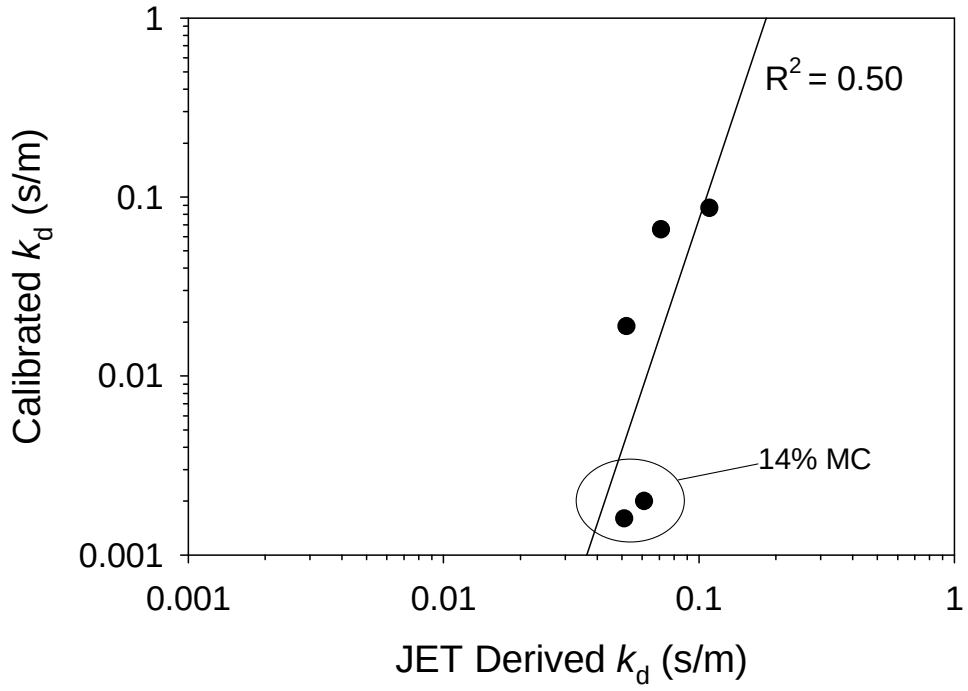

Figure 3-5. Regression between the erodibility coefficients (k_d) derived from JETs and those predicted from calibrating the Bonelli et al. (2006) model to flow data.

CHAPTER IV

CONCLUSIONS AND FUTURE WORK

Streambank erosion mechanisms are difficult to predict and quantify. This research attempted to quantify seepage erosion and soil piping in more cohesive soils and use models calibrated with observed data to predict erosion occurrences and quantification. Seepage and pipe erosion in the field is difficult to predict due to the presence of other contributing environmental factors. By utilizing uniform parameters such as density and moisture content, the process is isolated and mechanics of the development of the erosion are more easily studied.

Seepage erosion in hillslopes, gullies and streambanks results in tension ("pop-out") failure when seepage forces are greater than soil resistance and shear strength is reduced from an increase in soil pore-water pressure or particle entrainment and mobilization resulting in undercutting and eventual mass-failure. Previous research proposed a demarcation point between these two failure mechanisms that was determined to be density dependent. In sands, the demarcation point was at a density of 1.3 Mg m^{-3} and in loamy sands at 1.5 Mg m^{-3}. This increasing trend was observed with more cohesive soils although the demarcation point was approximately equivalent for the two sandy loam soils with varying clay content at 1.6 Mg m^{-3}. Undercutting shapes in both

sand and loamy sand soils were more focused at the center of the soil box with particle entrainment that resulted in less wide and deeper undercuts. Undercutting in sandy loam soils was much wider and typically extended the entire distance across the face of the soil box. Also, the undercutting process typically occurred as a set of smaller mass failures as the soil became saturated and eventually destabilized the bank to the point where one much larger mass-failure occurred. While failures were observed in the laboratory, SEEP/W and SLOPE/W were unsuccessful at predicting failures as SLOPE/W only considered pore-water pressures in its stability analysis and neglected seepage gradient forces.

Soil piping plays a significant role in a number of geomorphological processes and therefore more research should be devoted to explain and model observations from this research. Laboratory pipeflow experiments demonstrated that improved deterministic models are needed to better simulate soil piping and internal erosion processes. In many cases, soil pipes erode so quickly that transport-limited conditions can be created, which may potentially lead to pipe clogging and the buildup of pore water pressures that can cause geotechnical failure. Also, model assumptions regarding the geometric structure of the pipe were violated. It was observed that simple geometries no longer represented cases in which the material quickly eroded and the pipe expanded preferentially at the bottom of the pipe cross-section where shear stresses were higher.

Future work to improve seepage and soil piping models should focus on the following:

1. Quantifying the effect of seepage gradient forces on the erosion process both in terms of undercutting at exit points on hillslopes and also within soil pipes. Relying only on pore-water pressure effects may not be accurate in predicting all the potential mechanisms of instability. Are gradients between a flowing soil pipe and the surrounding soil material sufficient to influence the erodibility of the soil pipe?
2. There is a need to develop fully integrated models capable of considering variably saturated flow, dynamic geometries, and geotechnical analyses for seepage erosion and piping/internal erosion. Strategies are needed to determine how to develop data sets to parameterize these models.

Investigating seepage and pipe erosion in a laboratory setting provides a controlled environment for study. This allows for factors such as uniform soil at a uniform bulk density and a lack of environmental factors such as roots, insects and other variables. Studying these processes in laboratory settings helps form a deeper understanding of the processes involved, without any outside factors. However, in order to obtain a true representation of streambank erosion, more laboratory and field experiments must be initiated with even more cohesive soils and conditional factors such as roots that could also play a role in helping or hindering streambank erosion.

REFERENCES

Al-Madhhachi, A. T., Hanson, G. J., Fox, G. A., Tyagi, A. K., and Bulut, R. 2012a. Measuring soil erodibility using laboratory “mini” JET tests. *Transactions of the ASABE* (in review).

Al-Madhhachi, A. T., Hanson, G. J., Fox, G. A., Tyagi, A. K., and Bulut, R. 2012b. Deriving parameters of a fundamental detachment model for cohesive soils from flume and Jet Erosion Tests. *Transactions of the ASABE* (in review).

Bonelli, S., Brivois, O., Borghi, R., and Benahmed, N. 2006. On the modeling of piping erosion. *C.R. Mecanique* 334: 555-559.

Bradford, J. M., and Piest, R. F. 1977. Gully wall stability in loess derived alluvium. *Soil Science Society of America Journal* 41(1): 115-122.

Chu-Agor, M. L., Fox, G. A., Cancienne, R. M., and Wilson, G. V. 2008a. Seepage caused tension failures and erosion undercutting of hillslopes. *Journal of Hydrology* 359 (3-4): 247-259.

Chu-Agor, M., Wilson, G. V., and Fox, G. A. 2008b. Numerical modeling of bank instability by seepage erosion. *Journal of Hydrologic Engineering* 13(12): 1133-1145.

Crosta, G., and di Prisco, C. 1999. On slope instability induced by seepage erosion. *Canadian Journal of Geotechnical Engineering* 36: 1056-1073.

Darby, S. E., Rinaldi, M., and Dapporto, S. 2007. Coupled simulations of fluvial erosion and mass wasting for cohesive river banks. *Journal of Geophysical Research* 112, F03022, doi: 10.1029/2006JF000722.

Fox, G. A., and Wilson, G. V. 2010. The role of subsurface flow in hillslope and streambank erosion: A review. *Soil Science Society of America Journal* 74: 717-733.

Fox, G. A., Sabbagh, G. J., Chen, W., and Russell, M. 2006. Uncalibrated modeling of conservative tracer and pesticide leaching to groundwater: Comparison of potential Tier II exposure assessment models. *Pest Management Science* 62(6): 537-550.

Fox, G. A., Wilson, G. V., Simon, A., Langendoen, E., Akay, O., and Fuchs, J. W., 2007. Measuring streambank erosion due to ground water seepage: correlation to bank pore water pressure, precipitation, and stream stage. *Earth Surface Processes and Landforms* 32(10): 1558-1573.

Fredlund, D. G., and Rahardjo, H. 1993. *Soil Mechanics of Unsaturated Soils*. New York, N.Y.: John Wiley and Sons, Inc.

Hanson, G. J. 1990. Surface erodibility of earthen channels at high stresses. II: Developing an in situ testing device. *Transactions of the ASAE* 33(1): 132-137.

Hanson, G. J., and Hunt, S. L. 2007. Lessons learned using laboratory jet method to measure soil erodibility of compaction soils. *Transactions of the ASABE* 23(3): 305-312.

Krahn, J. 2004a. Seepage modeling with SEEP/W: An engineering methodology. GEO-SLOPE International Ltd. Calgary, Alberta, Canada.

Krahn, J. 2004b. Stability modeling with SLOPE/W: An engineering methodology. GEO-SLOPE/W International Ltd. Calgary, Alberta, Canada.

Lambe, T. W. 1962. Soil Stabilization. Chap. 4 of Foundation Engineering, G. A. Leonards, Ed., McGraw-Hill, New York.

Lobkovsky, A. E., Jensen, B., Kudrolli, A., and Rothman, D. H., 2004. Threshold phenomena in erosion driven by subsurface flow. *Journal of Geophysical Research-Earth Surface* 109(F4), F04010.

McWhorter, D. B., and Sunada, D. K. 1977. Ground-Water Hydrology and Hydraulics. *Water Resources Publications*. Fort Collins, CO. pg. 79-80.

Midgley, T. L., Fox, G. A., Wilson, G. V., Heeren, D. M., Langendoen, E. J., and Simon, A. 2012a. Streambank erosion and instability induced by seepage: In-situ injection experiments. *Journal of Hydrologic Engineering* (in press).

Midgley, T. L., Fox, G. A., Wilson, G. V., Felice, R. M., and Heeren, D. M. 2012b. In-situ soil pipeflow experiments on contrasting streambank soils. *Transactions of the ASABE* (in review).

Pierson, T. C. 1983. Soil pipes and slope stability. *Quarterly Journal of Engineering Geology and Hydrogeology* 16:1-11.

Regazzoni, P. L., Hanson, G. J., Wahl, T., Marot, D., and Courivaud, J. R. 2008. The

influence of some engineering parameters on the erosion of soils. *Fourth International Conference on Scour and Erosion (ICSE-4)*, Tokyo, Japan, November 5-7, 2008.

Rhoades, P. R., Oldham, L., and Wilson, G. V. 2007. Data compilation for Conservation Effects Assessment Project: Yalobusha River Watershed, Final Report. USDA-ARS National Sedimentation Laboratory Technical Report No. 51, Oxford, MS, p 1-169.

Tomlinson, S.S., and Vaid, Y.P. 2000. Seepage forces and confining pressure effects on piping erosion. *Canadian Geotechnical Journal* 37(1): 1-13.

Uchida, T., Kosugi, K., and Mizuyama, T. 2001. Effects of pipeflow on hydrological process and its relation to landslide: a review of pipeflow studies in forested headwater catchments. *Hydrological Processes* 15: 2151-2174.

van Genuchten, M. Th., Leij, F. J., and Yates, S. R. 1991. The RETC Code for Quantifying the Hydraulic Function of Unsaturated Soils. United States Environmental Protection Agency (USEPA) 000/091/000, USEPA, Ada, OK.

van Genuchten, M. T. 1980. A closed-form equation for predicting the hydraulic conductivity of unsaturated soils. *Soil Science Society of America Journal* 44(5): 892-898.

Wan, C. F., and Fell, R. 2004. Laboratory test on the rate of piping erosion of soils in embankment dams. *Geotechnical Testing Journal* 27(3): 295-303.

Whitlow, R. 1983. Basic Soil Mechanics. Construction Press, New York.

Wilson, C. G., Kuhnle, R.A., Bosch, D. D., Steiner, J. L., Starks, P. J., Tomer, M. D., and Wilson, G. V. 2008. Quantifying relative contributions from sediment sources in

Conservation Effects Assessment Project watersheds. *Journal of Soil and Water Conservation* 63(6): 523-531.

Wilson, G. V. 2009. Mechanisms of ephemeral gully erosion caused by constant flow through a continuous soil-pipe. *Earth Surface Processes and Landforms* 34: 1858-1866.

Wilson, G. V. 2011. Understanding soil-pipeflow and its role in ephemeral gully erosion. *Hydrological Processes* 25: 2354-2364.

Wilson, G. V., and Fox, G. A. 2013. Pore-water pressures associated with clogging of soil pipes: Numerical analysis of laboratory experiments. *Soil Science Society of America Journal* (in review).

Wilson, G. V., Nieber, J., Sidle, R. C., and Fox, G. A. 2012. Internal erosion during pipeflow: Review of experimental and numerical approaches. *Transactions of the ASABE* (in press).

Wilson, G. V., Periketi, R., Fox, G. A., Dabney, S., Shields, D., Cullum, R. F. 2007. Seepage erosion properties contributing to streambank failure. *Earth Surface Processes and Landforms* 32(3): 447-459.

VITA

Type Rachel Gayle Felice

Candidate for the Degree of

Master of Science

Thesis: LABORATORY INVESTIGATIONS OF THE MECHANISMS OF GROUNDWATER SEEPAGE EROSION AND PIPING IN COHESIVE SOILS

Major Field: Biosystems Engineering

Biographical:

Education:

Completed the requirements for the Master of Science in Biosystems Engineering at Oklahoma State University, Stillwater, Oklahoma in December, 2012.

Completed the requirements for the Bachelor of Science in Biosystems Engineering at Oklahoma State University, Stillwater, Oklahoma in May, 2010.

Experience: U.S. Army Corps of Engineers Student Career Experience Program Participant in Tulsa, OK; Graduate Research Assistant at Oklahoma State University, Biosystems Engineering Department Recruiter at Oklahoma State University; Environmental Intern at GE Aviation in Arkansas City, KS; Engineering Intern at Woolpert, LLP in Columbia, SC; Woolpert Research Scholar at Oklahoma State University

Professional Memberships: American Society of Agricultural and Biological Engineers